Analyst

PAPER

View Article Online
View Journal

Cite this: DOI: 10.1039/d5an01102g

A dual-modal ^{19}F MRI/^{18}F PET approach using sultone-derived chemical tags

Amaury Guillou,[a] Nicolas Joudiou,[b] Alice Fortin,[a] Fabienne Gourand,[a] Lionel Mignion,[b] Bénédicte F. Jordan,[c] Dominique Cahard[d] and Cécile Perrio*[a]

Received 18th October 2025,
Accepted 2nd February 2026

DOI: 10.1039/d5an01102g

rsc.li/analyst

Biocompatibility and hydrophilicity are key factors in the design of water-soluble imaging probes, particularly for ^{19}F MRI, where perfluorocarbon contrast agents are typically highly hydrophobic. To address this limitation, two original sultones containing a polyfluorinated pentaerythritol scaffold were developed and evaluated as precursors of hydrophilic and sensitive ^{19}F MRI tags. Their ring opening with $^{19/18}$F-fluoride led quantitatively to the corresponding polyfluorinated sulfo compounds that demonstrated water-solubility properties suitable for formulation and *in vivo* injection. ^{19}F MRI studies in mice, performed with unprecedented low doses (<100 μM) of the stable polyfluorinated sulfo compounds, provided high-contrast whole-body images consistent with PET imaging of their radiofluorinated analogues. These findings demonstrate that polyfluorinated sultones are promising chemical precursors for ^{19}F MRI and dual ^{19}F MRI/^{18}F PET probes, enabling improved diagnostic performance.

Introduction

Fluorine magnetic resonance imaging (^{19}F MRI) is an evolving research area with high potential to advance the fields of biomedical and diagnostic investigations.[1,2] Thanks to its high magnetic resonance (MR) intrinsic sensitivity, 83% of that of ^{1}H, along with its gyromagnetic ratio, 100% natural abundance, and negligible presence in biological tissues, the ^{19}F nucleus produces a distinct and isolated signal in MRI. This enables precise *in vivo* tracking of biological targets using suitable exogenous fluorinated probes.[3,4] Thus, ^{19}F MRI can offer quantitative images without tissue depth limitations and background interference. Compatible with the same MRI equipment after software and pulse sequence adjustments, ^{19}F MRI effectively complements the widely used, high resolution ^{1}H MRI. Combining both techniques allows functional and metabolic information to be associated with anatomical details. However, the use of ^{19}F MRI is hampered by a low *in vivo* sensitivity and a lack of suitable imaging agents that are soluble in water and biocompatible. Detectable ^{19}F MR signals require fluorine nuclei to be present at millimolar concentrations. This is typically achieved by designing probes that possess a large number of NMR equivalent fluorine atoms to enhance the ^{19}F signal, often through multiple trifluoromethyl (CF_3) groups.[5–7] PERFECTA, a tetrabranched superfluorinated compound featuring a pentaerythritol core (Fig. 1), exhibits highly favourable chemical and structural properties for enhancing ^{19}F-MRI imaging sensitivity. Its four perfluoro-*tert*-butoxy units provide 36 symmetrically distributed, magnetically equivalent fluorine atoms, resulting in an intense ^{19}F MRI signal at a distinct chemical shift of approximately −73 ppm.[8] However, due to the extreme hydrophobicity of perfluorocarbon structures, PERFECTA can only be used in encapsulated or emulsion formulations within biocompatible nanovectors, enabling *in vivo* administration and ensuring favorable pharmacokinetics.[9,10] In the same vein, ^{19}FIT (^{19}F imaging tracer, Fig. 1) has been reported as a water dispersible waxy compound able to form injectable micelles in physiological buffer solutions without requiring complex formulation procedures.[11] ^{19}FIT was designed as a bispherical cone, with three fluorinated branches forming a sphere that contains 27 equivalent fluorine atoms (nine CF_3 groups), which generate a single intense ^{19}F signal around −71 ppm. The second sphere, made of four polyethylene glycol (PEG) chains, served to enhance the aqueous solubility of the tracer. Phantom MRI experiments at 3 T showed a detection limit of approximately 125 mM ^{19}F atom concentration. *In vivo* imaging after intravenous (i.v.) injection in mice was successful, showing a residence half-life of about 0.5 days with no sign of organ retention or degra-

[a]*CNRS, CEA, Normandie Université, UAR 3408, Cyceron, Bd Henri Becquerel, 14074 Caen, France. E-mail: perrio@cyceron.fr*
[b]*UCLouvain, Nuclear and Electron Spin Technologies, NEST, Avenue Mounier 73.08, Woluwe-Saint-Lambert 1200, Belgium*
[c]*UCLouvain, Biomedical Magnetic Resonance Unit (REMA), Avenue Mounier 73.08, Woluwe-Saint-Lambert 1200, Belgium*
[d]*CNRS, UMR 6064 CARMeN, Normandie Université, 76821 Mont Saint Aignan, France*

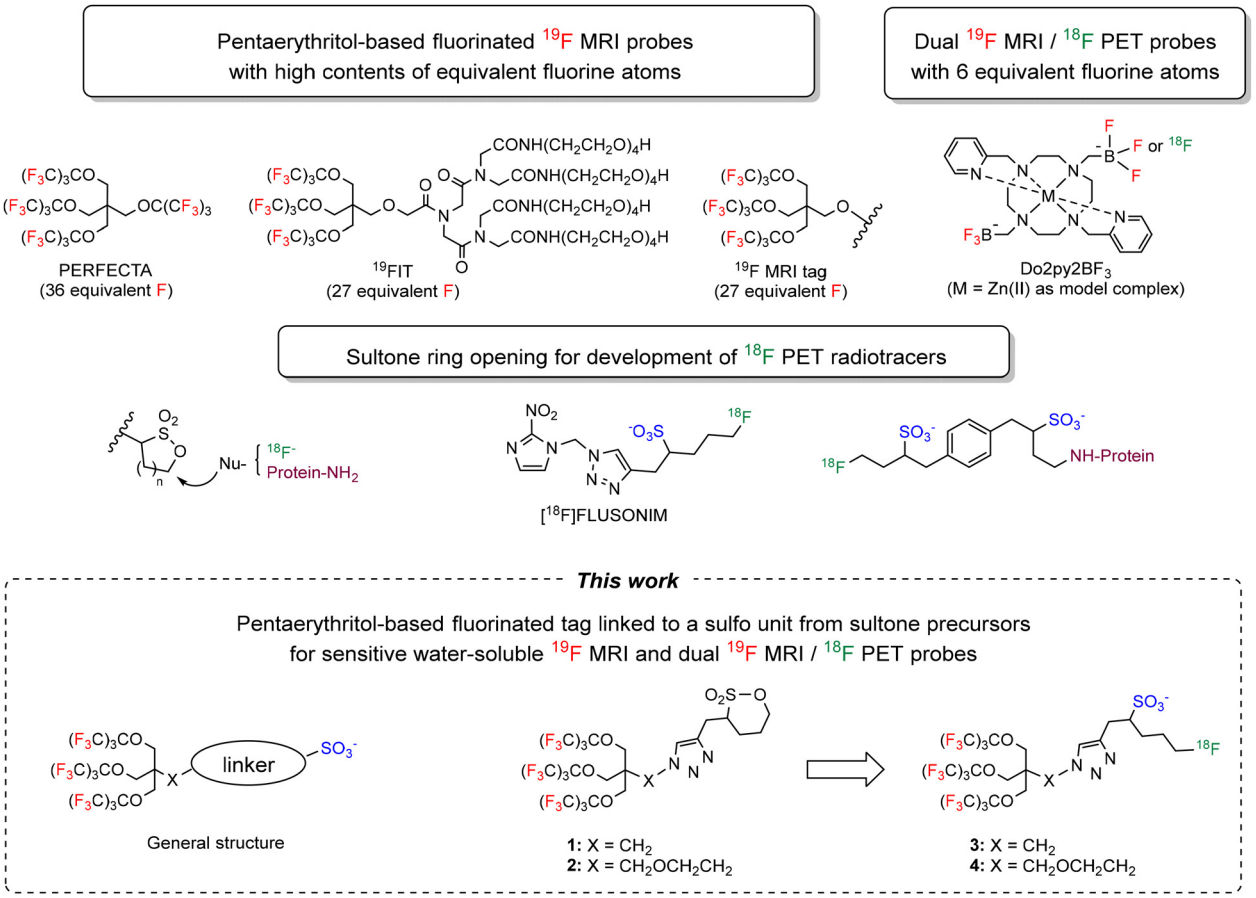

Fig. 1 Rationale of the work.

dation. As a result, ^{19}FIT addresses major limitations of traditional perfluorocarbons, including heterogeneity, instability, split ^{19}F signals, complex formulation procedures, and prolonged organ retention lasting months or more. However, ^{19}FIT, as it stands, could not provide any specific targeting. To this end, the tri-branched fluorinated pentaerythritol motif, offering a strong ^{19}F MR signal, has been successfully exploited as a ^{19}F MRI tag for vectorised nanomaterials, with grafting being performed at the unsubstituted pentaerythritol alcohol group.[12] Moreover, such a hydrophobic tag may negatively affect the physicochemical properties, pharmacokinetics and specific biological target recognition. Recently, the methylene trifluoroborate (CH_2BF_3) group has been proposed as an alternative to trifluoromethyl units in the azamacrocyclic chelating structure.[13] With two equivalent BF_3 entities, a single ^{19}F MR signal was detected at −137 ppm. However, the macrocycle structure suffers from great lipophilicity, preventing its solubility in physiological medium, and no *in vivo* evaluation was reported. In addition, the macrocycle lacks conjugation sites, and introducing a functional group for conjugation can disrupt its symmetry. This loss of symmetry may alter and multiply the chemical shifts, ultimately leading to blurred MR images. Nevertheless, the presence of BF_3 units opens the way to the development of radiotracers for positron emission tomography (PET) imaging by ^{19}F/^{18}F exchange. Unlike ^{19}F MRI, PET is a highly sensitive molecular imaging technique.[14] PET operates on the principle of detecting high energy photon pairs emitted by annihilation of positrons with electrons, which facilitates the quantification but provides poor spatial resolution. Based on dose tracer administration of a radiopharmaceutical labelled with a positron emitter, PET faces inherent limitations that include ionizing radiation, short half-life tracers and high cost. However, fluorine-18 is a highly attractive positron emitter radioisotope due to its favourable physical properties ($t_{1/2}$ = 109.7 min, 97% β^+ emission purity, 635 keV positron energy), its efficient production, and its well-developed radiochemistry, allowing centralized, large-scale preparation and off-site distribution of radiopharmaceuticals.[15] As PET and ^{19}F MRI present distinct limitations, their combined use could be a means to increase robustness in the diagnostic accuracy. PET can be used for rapid assessment of target distribution, helping to determine where higher resolution MR images should be taken to identify regions of interest. ^{19}F MRI, which uses stable imaging agents that can be stored for extended periods, could serve as a follow-up imaging method after radioisotope decay. Thus, chemical tags offering dual-modal ^{19}F MRI and ^{18}F PET imaging have emerged as an advantageous solution for further investigations.[16] Indeed,

dual tags open the way to PET-guided ^{19}F MRI follow-up imaging, with PET providing very high sensitivity and rapid whole-body assessment at tracer doses, allowing the identification of biodistribution and regions of interest, and ^{19}F MRI enabling background-free and long-term imaging using stable probes. Such a complementary multimodal imaging strategy can therefore be beneficial for pharmacokinetic studies as well as for increasing robustness and interpretability in preclinical imaging approaches. However, their design to achieve high performance ^{19}F MRI agents with high sensitivity, suitable physicochemical features, water solubility, biocompatibility, excellent pharmacokinetics and biological properties, and labelling with fluorine-18, remains a major concern.

Besides grafting PEG chains, the introduction of a negatively charged sulfonate (sulfo) group is a well-known approach for adding hydrophilicity.[17] This strategy is widely encountered, for example, in the field of aromatic dyes for optical imaging.[18] An easy way to access sulfo dyes is through the nucleophilic attack of an amine or phenolate group present in the dye on propane sultone.[19] We recently extended sultone chemistry to the development of PET radiotracers.[20] We found that functionalized propane and butane sultones were prone to ring-opening by cyclotron-produced ^{18}F-fluoride to afford ^{18}F-sulfo compounds endowed with optimized physicochemical properties for *in vivo* imaging as well as for bio-conjugation applications.[21–23] As a representative example, the radiotracer [^{18}F]FLUSONIM (Fig. 1) was designed for tumour hypoxia PET imaging and demonstrated high contrast along with fast background clearance due to its highly hydrophilic properties.[21] We also took advantage of the sultone reactivity toward fluoride and amines to carry out ^{18}F-radiolabeling of proteins and glycoproteins at the lysine amino residues under biocompatible conditions according to two sequential ring opening reactions (*i.e.* radiofluorination then amination) from a bis-sultone.[23] In this context, we envisioned the design of appropriate sultones as precursors of new ^{19}F-MRI sulfo tags that associate, through a linker, the tris(perfluoro-*tert*-butyl) pentaerythritol scaffold to an anionic sulfonic unit (Fig. 1). The sulfo group polarity could offset the hydrophobic polyfluorinated moiety in order to obtain biocompatible probes with fine-tuned physicochemical properties. The linker would allow the sulfo group to be distanced from the perfluorinated unit and the ^{19}F-MRI sulfo tags to be distinguished from the PFOS (perfluorooctanesulfonic acid) class of compounds that is now being challenged for environmental reasons.[24] Herein, we present the synthesis of the polyfluorinated sultones **1** and **2** possessing a triazolyl linker that also contribute to enhancing hydrophilicity,[25] and their (radio)fluorination as an application of the sultone ring-opening strategy. The resulting $^{19/18}$F-sulfonates **3** and **4** were evaluated as biocompatible chemical labels by PET and ^{19}F MRI in healthy animals. The obtained images were compared, providing information on the *in vivo* behaviour of the sulfo tags in the radioactive and non-radioactive forms (*i.e.* stability, pharmacokinetics, biodistribution and elimination), and also proof of concept for dual ^{19}F MRI/PET tagging.

Results and discussion

Chemistry

Polyfluorinated sultones **1** and **2** were prepared according to a three-step synthesis starting from previously described tris (perfluoro-*tert*-butyl) pentaerythritol **5** and its hydroxypropyl elongated derivative **6** (Scheme 1).[26,27]

Mesylation of alcohols **5** and **6** followed by displacement with sodium azide furnished azides **7** and **8** in 70 and 98% yields, respectively. Azides **7** and **8** were then transformed *via* a copper(I)-catalyzed azide–alkyne cycloaddition (CuAAC) reaction with the propargylic butane sultone[21] using CuI in DMF at 55 °C for 24 h to obtain the desired sultones **1** and **2** in 81 and 73% yields, respectively. Finally, the nucleophilic ring opening fluorination of sultones **1** and **2** led almost quantitatively to fluorosulfonates **3** and **4** by means of TBAF in a refluxing acetonitrile solution for 48 h or in a refluxing DMF solution for 24 h (Scheme 1). ^{19}F NMR spectra of compounds **3** and **4** (performed using hexafluoroisopropanol (HFIP) as an internal standard, δ = −77.3 ppm) displayed a single, intense signal at approximately −72 ppm for the 27 equivalent fluorine atoms and a small signal at −220 ppm for the lonely fluorine atom. These results highlight the efficiency of the synthetic sequence: in only three steps, the targeted polyfluorinated sultones were obtained in good yields and then quantitatively converted into the corresponding fluorosulfonates. The strategy thus proved to be both robust and versatile, relying on simple transformations to deliver the desired compounds with high selectivity and purity. The next steps will involve assessing the radiochemistry and properties of fluorosulfonates **3** and **4** to confirm their relevance for the intended applications.

Radiochemistry

The radiosyntheses of ^{18}F-fluorosulfonates [^{18}F]**3** and [^{18}F]**4** were performed on a GE TRACERLab FXFN automated system from dried [^{18}F]TBAF obtained after trapping cyclotron produced ^{18}F-fluoride (recovered in ^{18}O-enriched water) on a QMA Sep-Pak cartridge, followed by elution with a solution of $TBAHCO_3$ in a mixture of water and acetonitrile, and finally azeotropic evaporation. Sultone **1** or **2** (8 mg) in an acetonitrile solution (1 mL) was added to the reactor containing dried [^{18}F]TBAF and heating was maintained at 100 °C for 30 min (Scheme 2). The radiolabelled fluorosulfonates [^{18}F]**3** and [^{18}F]**4** were isolated after purification by reversed-phase semi-preparative HPLC using an 80/20 (v/v) acetonitrile/water (with 0.1% TFA) mixture as an eluent, then formulated through reverse phase SPE in a saline solution containing ethanol (7–8%). Radiochemical conversions (RCCs) for radiofluorinations were greater than 90% as revealed on the semi-preparative HPLC chromatograms in Scheme 2. These results once again demonstrate the high efficiency of the ring-opening reaction of butane sultones with ^{18}F-fluoride. The formulation step, although time consuming, enabled recovery of approximately 50–70% of the ^{18}F-fluorosulfonates [^{18}F]**3** and [^{18}F]**4** after HPLC purification, indicating potential biocompatibility.

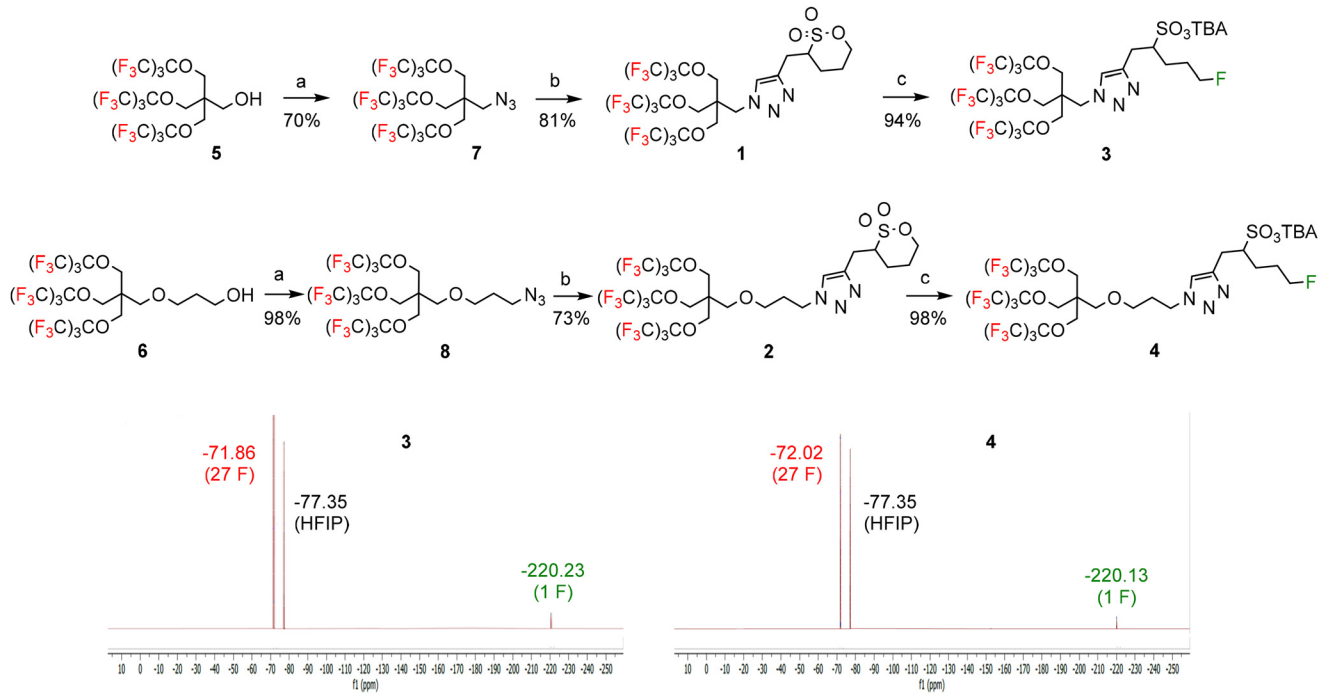

Scheme 1 Synthesis and ^{19}F NMR spectra (with HFIP as an internal standard) of target probes **3** and **4**. Reagents and conditions: (a) MsCl, Et_3N, CH_2Cl_2, rt, 48 h; then NaN_3, DMF, 60 °C for 76 h for **7**, 80 °C for 48 h for **8**; (b) propargylic butanesultone, CuI, DMF, 55 °C, 24 h; and (c) TBAF, CH_3CN at reflux for 48 h or DMF at reflux for 24 h.

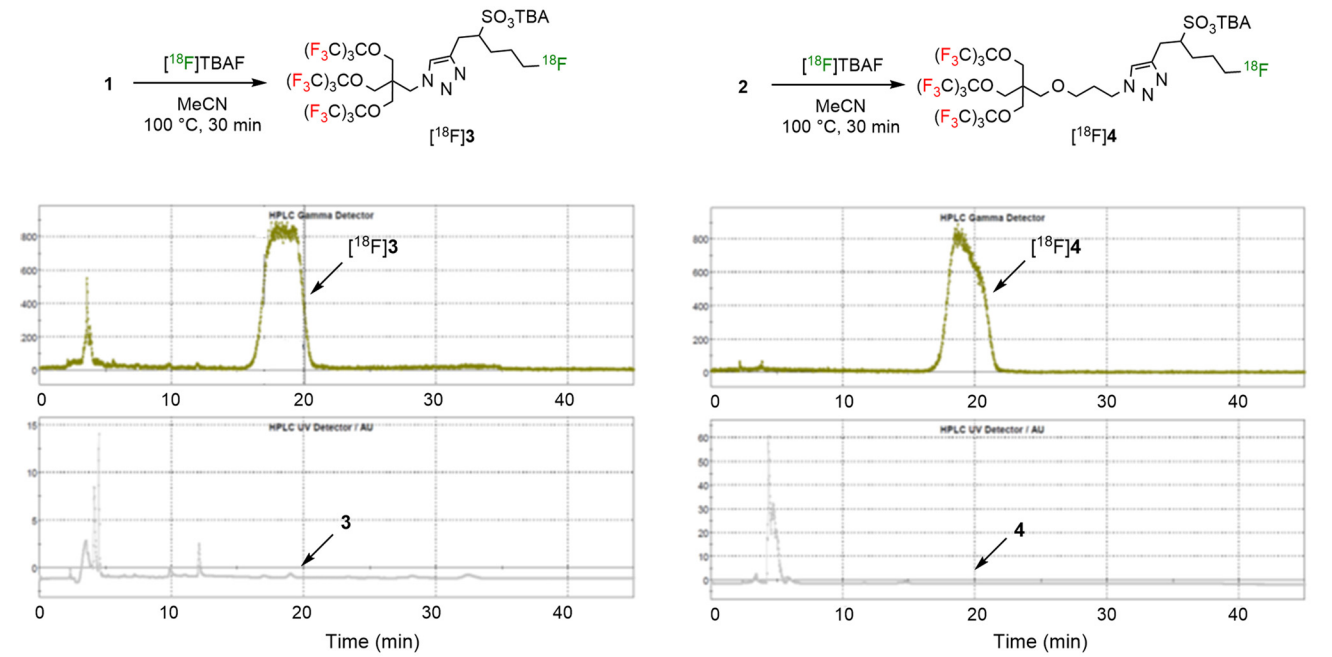

Scheme 2 Radiosynthesis of [^{18}F]**3** and [^{18}F]**4**.

The activity yields for [^{18}F]**3** and [^{18}F]**4** were 18–25% and 12–18% (n = 5), respectively, after 75 min total synthesis time (including purification and formulation steps). The identity of ^{18}F-fluorosulfonates [^{18}F]**3** and [^{18}F]**4** was confirmed by comparison of reverse phase analytical HPLC of the formulation solutions (radioactive detection) and of the non-radioactive products **3** and **4** (see UV traces in Fig. 2A and B). Both radioHPLC and radioTLC analyses of ^{18}F-fluorosulfonates [^{18}F]

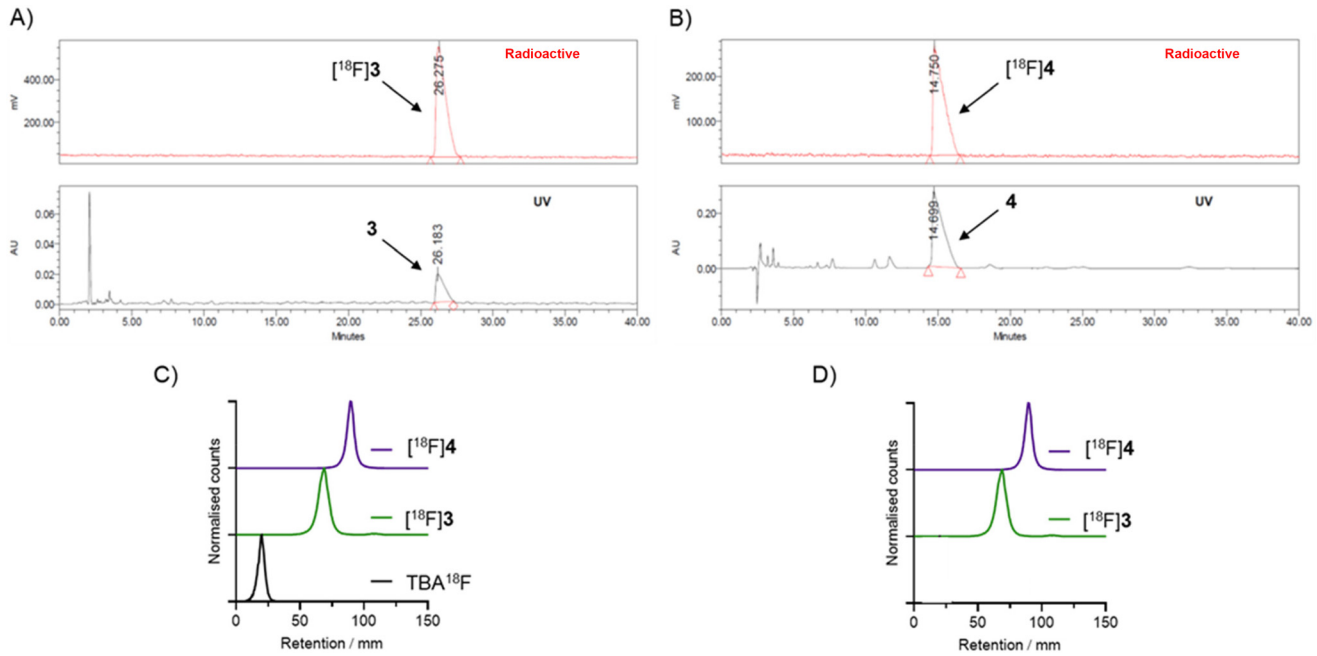

Fig. 2 Characterization by analytical radioHPLC of formulated [^{18}F]**3** (A, top) and [^{18}F]**4** (B, top) by comparison with HPLC (UV) of references **3** (A, bottom) and **4** (B, bottom), and radioTLC analysis of [^{18}F]**3** and [^{18}F]**4** in the formulated solution (C) and after incubation at 37 °C for 2 h in human serum (D).

3 and [^{18}F]**4** revealed high radiochemical purity (>99%) and a molar activity of >200 GBq μmol^{-1} (>5 Ci μmol^{-1}).

Hydrophilicity and *in vitro* stability

The hydrophilicity of [^{18}F]**3** and [^{18}F]**4** was evaluated by the experimental determination of octanol/water and octanol/buffer (pH 7.4) partition coefficient values, log *P* and log $D_{7.4}$, respectively. [^{18}F]**3** exhibits a log *P* value of 2.30 ± 0.05 and log $D_{7.4}$ = 1.95 ± 0.05 (n = 9). The values for [^{18}F]**4** are slightly higher with log *P* = 2.85 ± 0.09 and log $D_{7.4}$ = 2.48 ± 0.02 (n = 9). These values, ranging from 2 to 3, demonstrate a predominantly lipophilic character for both [^{18}F]**3** and [^{18}F]**4**, with [^{18}F]**4** being a little more lipophilic than [^{18}F]**3** in accordance with the presence of the oxypropylene chain. However, they remain compatible with *in vivo* applications and they comply with the capacity for [^{18}F]**3** and [^{18}F]**4** to be solubilized in aqueous medium containing <10% ethanol for formulation. The charged sulfonate group in [^{18}F]**3** and [^{18}F]**4** greatly counterbalances the highly hydrophobic tris(perfluoro-*tert*-butyl) pentaerythritol backbone.

The *in vitro* stability of [^{18}F]**3** and [^{18}F]**4** was evaluated by radioTLC after incubation at 37 °C in human serum. After 2 h, [^{18}F]**3** and [^{18}F]**4** were recovered totally unchanged (Fig. 2C and D). No signs of degradation or chemical modification were detectable, indicating that [^{18}F]**3** and [^{18}F]**4** retained their integrity under physiological conditions.

PET and ^{19}F MRI experiments

In order to compare PET and ^{19}F MRI, probes [^{18}F]**3** and [^{18}F]**4** were first evaluated in healthy SWISS mice by dynamic whole body PET imaging over 30 min to assess the pharmacokinetics, biodistribution and elimination. PET was coupled to anatomic ^{1}H MRI for image registration, and time–activity curves (TAC) were determined (Fig. 3). For both probes [^{18}F]**3** and [^{18}F]**4** administered at tracer doses by i.v. injection in the tail vein, the radioactivity was rapidly distributed within the first minute, throughout the body, with the highest concentration observed in the liver, where the mean standard uptake values (SUV_{mean}) reached around 7 at 1 min. The radioactivity uptake was much lower in the other main organs, with the order of uptake being as follows: heart ($SUV_{mean} \approx 5$), lungs ($SUV_{mean} \approx 2$) and kidneys ($SUV_{mean} \approx 1$). From 2 min, accumulation of [^{18}F]**3** and [^{18}F]**4** remained high and stable in the liver with SUV_{mean} values of 10–11 that remained constant until the end of the acquisition (30 min). The radioactivity levels declined dramatically in the heart as well as in the lungs and kidneys, with SUV_{mean} values down to around 1 at 2 min, showing no retention of both [^{18}F]**3** and [^{18}F]**4** in those organs. No uptake was observed in muscle (SUV_{mean} near 0), and penetration into the brain was non-existent, meaning no crossing of the blood–brain barrier. Thus, the two probes [^{18}F]**3** and [^{18}F]**4** were almost exclusively accumulated in the liver, with no noticeable difference between them. This hepatic retention remained stable for up to 30 minutes without significant uptake in the other organs (heart, lungs, and kidneys) and without renal elimination. The latter results are in agreement with the lipophilic nature of the probes.

Probes **3** and **4** were then evaluated in healthy SWISS mice by fluorine MRI also coupled to anatomical ^{1}H MRI (Fig. 3). They were easily formulated in an aqueous physiological saline solution containing 10% ethanol at a concentration of 30 mg

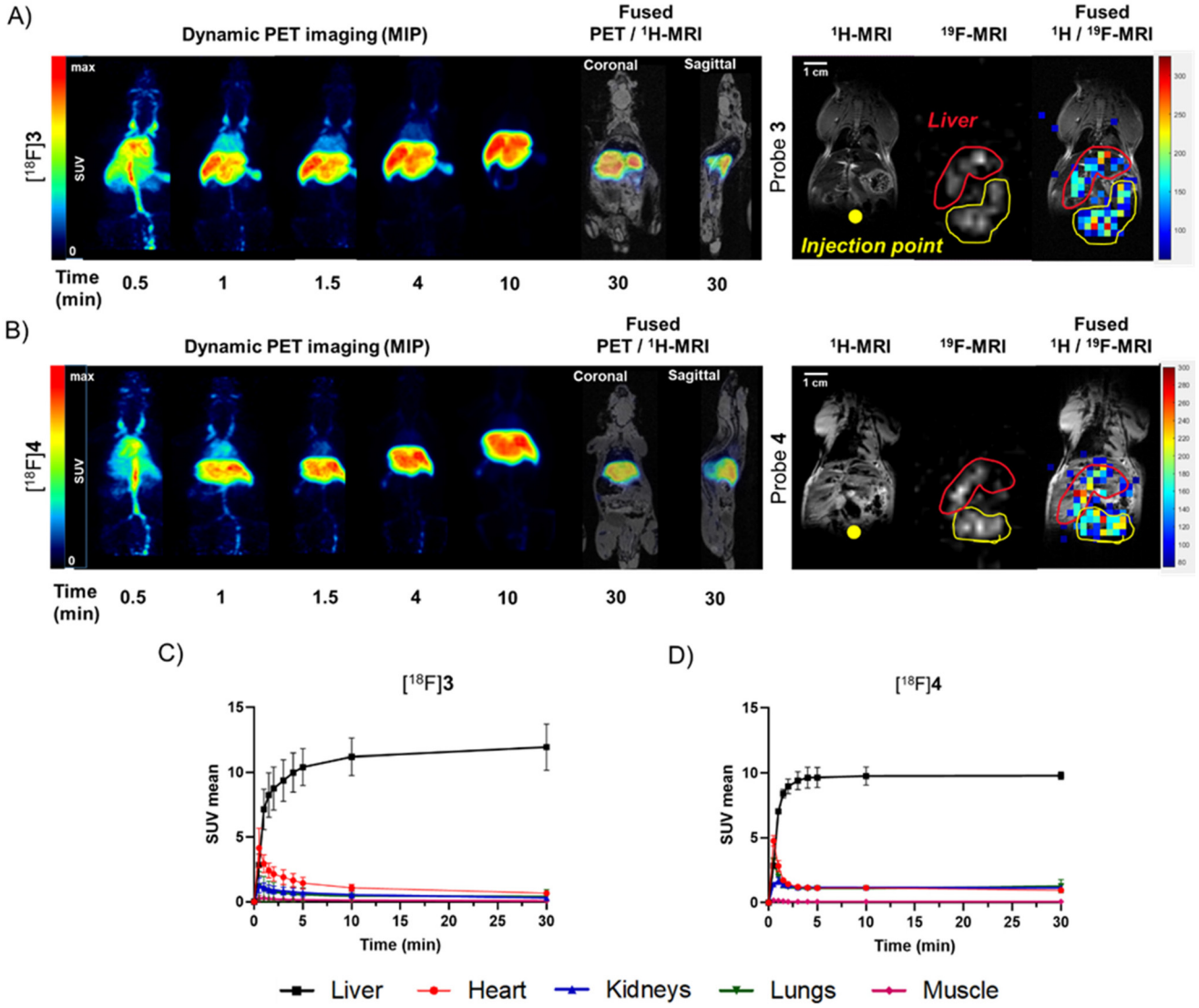

Fig. 3 Whole body PET and $^{1}H/^{19}F$ MRI in healthy mice after injection of [^{18}F]**3** or **3** (A) and [^{18}F]**4** or **4** (B), and time–activity curves (TACs) for the main organs (C and D, n = 3).

mL^{-1}, and they were administered by intraperitoneal injection at a dose of 3 mg for **3** and 2.3 mg for **4** (<100 μL of the parent solution), corresponding to approximately 50–75 μM ^{19}F atom concentrations. Based on the PET results, ^{19}F MR images were registered 20–40 min after injection using a FLASH ^{19}F sequence (TR: 150 ms, TE: 1.7 ms, FA: 30°, NEX: 128, total acquisition time: 10 min 14 s, in-plane resolution: 1.87 × 1.87 mm^2, slice thickness: 10 mm). Despite a low *in vivo* sensitivity, ^{19}F MR images clearly showed a signal in the peritoneal cavity, around the injection zone, with exclusive accumulation of the probes in the liver, consistent with PET imaging findings. Thus, ^{19}F MRI enabled the detection of probes **3** and **4** at injected doses on the order of ~0.1 mmol kg^{-1}, which are within the lower range of values reported for fluorinated MRI probes, including ^{19}FIT.[11] Thanks to PET imaging results, the absence of signals in other regions in the ^{19}F imaging was definitively assigned to the absence of probes and not to a lack of detection due to a too low MRI sensitivity. Such an example illustrates the added value of PET imaging in the development of ^{19}F MRI probes. Overall, the present work establishes a sultone-based chemical strategy for constructing well-defined biocompatible polyfluorinated tags that enable ^{19}F MRI and also true bimodal ^{18}F PET/^{19}F MRI imaging, opening up new opportunities for the development of targeted probes combining the sensitivity of PET with the background-free and long-term nature of ^{19}F MRI.

Conclusions

In this study, we investigated the association of a polyfluorinated pentaerythritol scaffold with a sulfonate moiety as a bio-

compatible and sensitive ^{19}F MRI tag. We developed two sulfo compounds **3** and **4** endowed with hydrophilic properties, allowing their simple formulation in a physiological medium containing 10% ethanol and *in vivo* administration, and we demonstrated that they exhibited comparable *in vivo* behavior. Both sulfo compounds, **3** and **4**, were efficiently radiolabelled with fluorine-18, enabling dual ^{18}F PET and ^{19}F MRI. The two imaging modalities produced consistent results, demonstrating accumulation of both labelled and unlabelled compounds in the liver, despite their moderate lipophilicity. In addition to the novelty of the double investigation by ^{18}F PET and ^{19}F MRI imaging, ^{19}F MRI could be realized using micromolar doses of sulfo compounds **3** and **4**. Overall, our results confirmed, once again, that sulfo tags offer advantages for *in vivo* imaging. They also illustrate the wide application field of the sultone ring opening reaction for developing biocompatible probes. Following this proof of concept for a biocompatible tag featuring a polyfluorinated pentaerythritol scaffold associated with a fluorosulfonate moiety, this methodology will be applied to the development of improved promising smart polyfluorinated entities for *in vivo* developments by ^{19}F MRI and dual PET/^{19}F MRI.

Author contributions

Conceptualization and funding acquisition by CP and DC; chemistry by AF; radiochemistry by FG and CP; PET imaging by AG, MRI by NJ, LM and BFJ; original draft by CP and DC; review and editing by all authors.

Conflicts of interest

There are no conflicts to declare.

Data availability

Supplementary information (SI): experimental procedures, spectroscopic data for characterization of the new compounds, and experimental details for ^{18}F-labeling, PET imaging and MRI experiments. See DOI: https://doi.org/10.1039/d5an01102g.

Acknowledgements

The authors thank CNRS, CEA, MESRI, Carnot I2C, the French National Agency for Research called "Investissements d'Avenir" Labex IRON (ANR-11-LABX-0018-01), and the European Union's Horizon 2020 research and innovation programme under the Marie Skłodowska-Curie Actions (grant agreement number 101034329) as well as the Normandy Region under the WINNINGNormandy program for financial support. B. F. Jordan is Research Director of the FRS/FNRS.

The animal investigations were performed under the current European directive (2010/63/EU) as incorporated in national legislations, and protocols were approved by the French (#47590) and Belgian (2024/UCL/MD/63) committees on animal ethics.

References

1 Y. Mo, C. Huang, C. Liu, Z. Duan, J. Liu and D. Wu, *Macromol. Rapid Commun.*, 2023, **44**, 2200744.
2 P. Yue, T. Nagendraraj, G. Wang, Z. Jinb and G. Angelovski, *Chem. Sci.*, 2024, **15**, 20122.
3 I. Tirotta, V. Dichiarante, C. Pigliacelli, G. Cavallo, G. Terraneo, F. Baldelli Bombelli, P. Metrangolo and G. Resnati, *Chem. Rev.*, 2015, **115**, 1106.
4 M. H. Cho, S. H. Shin, S. H. Park, D. K. Kadayakkara, D. Kim and Y. Choi, *Bioconjugate Chem.*, 2019, **30**, 2502.
5 L. L. Gervits, A. L. Sigan, A. A. Markova, M. V. Gulyaev, O. S. Pavlova, R. M. Ozhiganov and Y. A. Pirogov, *ChemMedChem*, 2023, **18**, e202300239.
6 L. Wu, F. Liu, S. Liu, X. Xu, Z. Liu and X. Sun, *Int. J. Nanomed.*, 2020, **15**, 7377.
7 L. Deing, G. Rong and Y. Cheng, *Macromol. Biosci.*, 2023, **23**, 2300048.
8 I. Tirotta, A. Mastropietro, C. Cordiglieri, L. Gazzera, F. Baggi, G. Baselli, M. G. Bruzzone, I. Zucca, G. Cavallo, G. Terraneo, F. Baldelli Bombelli, P. Metrangolo and G. Resnati, *J. Am. Chem. Soc.*, 2014, **136**, 8524.
9 D. Janasik and T. Krawczyk, *Chem. – Eur. J.*, 2022, **28**, e202102556.
10 L. Jamgotchian, S. Vaillant, E. Selingue, A. Doerflinger, A. Belime, M. Vandamme, G. Pinna, W. L. Ling, E. Gravel, S. Mériaux and E. Doris, *Nanoscale*, 2021, **13**, 2373.
11 Z.-X. Jiang, X. Liu, E.-K. Jeong and Y. Yu, *Angew. Chem., Int. Ed.*, 2009, **48**, 4755.
12 V. Dichiarante, I. Tirotta, L. Catalano, G. Terraneo, G. Raffaini, M. R. Chierotti, R. Gobetto, F. Baldelli Bombelli and P. Metrangolo, *Chem. Commun.*, 2017, **53**, 621.
13 C. Sire, V. Meneyrol, N. Saffon-Merceron, E. Terreno, F. Garello, L. Tei, E. Jestin, R. Tripier and T. Troadec, *Chem. Sci.*, 2024, **15**, 13550.
14 J. Schwenck, D. Sonanini, J. M. Cotton, H.-G. Rammensee, C. la Fougère, L. Zender and B. J. Pichler, *Nat. Rev. Cancer*, 2023, **23**, 474.
15 N. S. Goud, R. K. Joshi, R. D. Bharath and P. Kumar, *Eur. J. Med. Chem.*, 2020, **187**, 111979.
16 (*a*) R. Zhao, D. Lan, B. Xia, M. Dong, J. Mu and Y. Zhao, *Small*, 2025, **21**, 2409713; (*b*) C. Wang, B. I. Leach, D. Lister, S. R. Adams, H. Xu, C. Hoh, P. McConville, J. Zhang, K. Messer and E. T. Ahrens, *J. Nucl. Med.*, 2021, **61**, 1146.
17 D. K. Han, K. D. Park and Y. H. Kim, *J. Biomater. Sci., Polym. Ed.*, 1998, **9**, 163.
18 (*a*) C. S. Mahanta, V. Ravichandiran and S. P. Swain, *ACS Appl. Bio Mater.*, 2023, **6**, 2995; (*b*) G. Pascual, S. K. Roy, G. Barcenas, C. K. Wilson, K. Cervantes-Salguero, O. M. Obukhova, A. I. Krivoshey, E. A. Terpetschnig, A. L. Tatarets, L. Li, B. Yurke, W. B. Knowlton, O. A. Mass,

R. D. Pensack and J. Lee, *Nanoscale*, 2024, **16**, 1206; (*c*) W. Pham, Z. Medarova and A. Moore, *Bioconjugate Chem.*, 2005, **16**, 735; (*d*) A. Kamkaewa and K. Burgess, *Chem. Commun.*, 2015, **51**, 10664.

19 (*a*) S. L. Niu, G. Ulrich, R. Ziessel, A. Kiss, P.-Y. Renard and A. Romieu, *Org. Lett.*, 2009, **11**, 2049; (*b*) H. C. Daly, G. Sampedro, C. Bon, D. Wu, G. Ismail, R. A. Cahill and D. F. O'Shea, *Eur. J. Med. Chem.*, 2017, **135**, 392.

20 S. Schmitt, C. Bouteiller, L. Barré and C. Perrio, *Chem. Commun.*, 2011, **47**, 11465.

21 C. Maingueneau, A.-E. Lafargue, S. Guillouet, F. Fillesoye, T. T. C. Pham, B. Jordan and C. Perrio, *JACS Au*, 2024, **4**, 3248.

22 J. Beaufrez, S. Guillouet, Y. Seimbille and C. Perrio, *Pharmaceuticals*, 2023, **16**, 636.

23 A.-E. Lafargue, C. Maingueneau, B. Bernay, A. Ejjoummany and C. Perrio, *ACS Omega*, 2025, **10**, 17983.

24 A. Ducatman, J. LaPier, R. Fuoco and J. C. DeWitt, *Environ. Health*, 2022, **21**, 51.

25 Q. Guan, S. Xing, L. Wang, J. Zhu, C. Guo, C. Xu, Q. Zhao, Y. Wu, Y. Chen and H. Sun, *J. Med. Chem.*, 2024, **67**, 7788.

26 Z.-H. Jiang and Y. B. Yu, *Tetrahedron*, 2007, **63**, 3982.

27 M. Rosati, A. Acocella, A. Pizzi, G. Turtù, G. Neri, N. Demitri, Nonappa, G. Raffaini, B. Donnio, F. Zerbetto, F. Baldelli Bombelli, G. Cavallo and P. Metrangolo, *Macromolecules*, 2022, **55**, 2486.